

NRG approach to the transport through a finite Hubbard chain connected to reservoirs

Akira OGURI and A. C. HEWSON¹

¹Department of Material Science, Osaka City University, Sumiyoshi-ku, Osaka 558-8585, Japan

¹Department of Mathematics, Imperial College, 180 Queen's Gate, London SW7 2BZ, UK

(Received December 9, 2004)

We study the low-energy properties of a Hubbard chain of finite size N_C connected to two noninteracting leads using the numerical renormalization group (NRG) method. The results obtained for $N_C = 3$ and 4 show that the low-lying eigenstates have one-to-one correspondence with the free quasi-particle excitations of a local Fermi liquid. It enables us to determine the transport coefficients from the fixed-point Hamiltonian. At half-filling, the conductance for even N_C decreases exponentially with increasing U showing a tendency towards the development of a Mott-Hubbard gap. In contrast, for odd N_C , the Fermi-liquid nature of the low-energy states assures perfect transmission through the Kondo resonance. Our formulation to deduce the conductance from the fixed-point energy levels can be applied to various types of interacting systems.

KEYWORDS: Kondo effect, Hubbard model, reservoir, Fermi liquid, quantum dot, numerical renormalization group

1. Introduction

Electron transport through finite systems, such as quantum dots, quantum wires, and atomic chains of nanoscale, is a subject of much current interest. In these systems, a number of phenomena have been predicted theoretically and some have already been successfully observed. The Kondo effect in quantum dots is one such example.^{1–4} Furthermore, recent experimental developments make it possible to examine the interplay of various effects which have previously only been studied in different fields of physics. For instance, in quantum dots, the interplay of the Aharonov-Bohm, Fano, Josephson, and Kondo effects under equilibrium and nonequilibrium situations have been studying intensively.^{5–7} The Luttinger-liquid behavior in quantum wires has also been an active field of investigation,^{8,9} and numerical developments have been reported recently for spinless fermions on a lattice.^{10,11}

We have previously considered the transport properties of a finite Hubbard chain of size N_C ($=1, 2, 3, \dots$) connected to two noninteracting leads, which is illustrated in Fig. 1, as a model for a series of quantum dots and materials on a nanometer scale. We have discussed an even-odd oscillatory behavior of the dc conductance at half-filling based on a perturbation expansion in powers of the Coulomb repulsion U .^{12–14} For even N_C , the conductance decreases with increasing U showing a tendency towards the development of a Mott-Hubbard insulator gap.^{12–14} The conductance deduced from the order U^2 self-energy was qualitatively correct. However, a more accurate treatment is needed to deal quantitatively with the large U regime, which is one of the aims of this paper.

In contrast, for odd N_C , the transmission probability through the Hubbard chain reaches the unitary-limit value at $T = 0$ when the system has the electron-hole and inversion symmetries. Physically there is a Kondo resonance situated at the Fermi level which enables the

perfect transmission take place for any value of U . The proof was given by taking all contributions in powers of U formally into account for the $N_C \times N_C$ matrix self-energy $\Sigma(\omega)$. The assumption we have made is; $\text{Re } \Sigma(0)$ is *not singular* and $\text{Im } \Sigma(0) = 0$ at $T = 0$.¹³ The local Fermi-liquid state satisfies this assumption,¹⁵ and historically the same assumption has been made by Langer and Ambegaokar in the derivation of the Friedel sum rule for interacting electrons.¹⁶ In the case of the single Anderson impurity corresponding to $N_C = 1$, the perturbation theory in powers of U describes the low-energy Fermi-liquid behavior,¹⁷ and is consistent with the exact Bethe ansatz^{18–20} and NRG^{21–23} results. The perturbation expansion in U works because the contributions from the low-energy processes, in which electrons hop into the reservoirs and away from the impurity, are included in the noninteracting Green's functions via the hybridization energy scale Γ_L and Γ_R , where $\Gamma_{L/R} = \pi \rho v_{L/R}^2$. The perturbation expansion is also convergent for $N_C > 1$.^{12–14} It would be of interest to have these results confirmed by a non-perturbative technique, which is the second aim of the work presented in this paper.

To tackle both these problems we apply the non-perturbative NRG approach to the low energy physics of the Hubbard chain, connected to non-interacting leads. In doing so we go beyond the earlier low order perturbational results for the even site chains, and we also derive a Fermi liquid picture for the odd site chains, without making the assumptions implicit in the perturbation theory. The NRG method has been applied successfully to the quantum dots for $N_C = 1$ and 2.^{24,25} In the present work we have applied the NRG method for the Hubbard chain with size $N_C = 3$ and 4, which seem to capture the essence of the even- and odd-size chains, respectively. The results show that the low-lying energy states have a one-to-one correspondence with the quasi-particles exci-

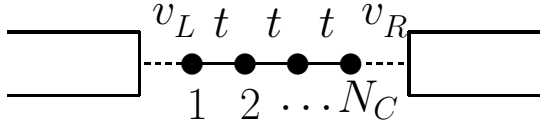


Fig. 1. Schematic picture of system.

tations of the local Fermi liquid. It assures the validity of the Fermi-liquid description at low energies. Specifically, for odd N_C , a number of the noninteracting sites are needed to be taken into account to reach the fixed point that describes the physics below the Kondo temperature T_K . The fixed point has much information about the low-temperature properties, and one can deduce the parameters such as T_K and Wilson ratio R from the flow of the eigenvalues.^{26,27} In the present paper, we provide a formulation to determine the conductance for even N_C at $T = 0$. For large U , the NRG method improves the perturbation results,¹³ and the conductance determined from the fixed-point energy levels decreases exponentially with increasing U .

In §2, we deduce expressions of the ground-state properties in terms of the Green's function. In §3, we describe the formulation to deduce the conductance from the fixed-point Hamiltonian. In §4, we show the NRG results. In §5, discussion and summary are given.

2. Model and Formulation

We consider a Hubbard chain of a finite size N_C situated at the center, which is attached to two non-interacting leads at the left (L) and the right (R). The complete Hamiltonian is given by

$$\mathcal{H} = \mathcal{H}_d + \mathcal{H}_U + \mathcal{H}_{\text{mix}} + \mathcal{H}_{\text{lead}}, \quad (1)$$

$$\begin{aligned} \mathcal{H}_d = & -t \sum_{i=1}^{N_C-1} \sum_{\sigma} \left(d_{i\sigma}^{\dagger} d_{i+1\sigma} + d_{i+1\sigma}^{\dagger} d_{i\sigma} \right) \\ & + \sum_{i=1}^{N_C} \left(\epsilon_d + \frac{U}{2} \right) n_{di}, \end{aligned} \quad (2)$$

$$\mathcal{H}_U = \frac{U}{2} \left(\sum_{i=1}^{N_C} n_{di} - 1 \right)^2, \quad (3)$$

$$\begin{aligned} \mathcal{H}_{\text{mix}} = & v_L \sum_{\sigma} \left(d_{1,\sigma}^{\dagger} \psi_{L\sigma} + \psi_{L\sigma}^{\dagger} d_{1,\sigma} \right) \\ & + v_R \sum_{\sigma} \left(\psi_{R\sigma}^{\dagger} d_{N_C,\sigma} + d_{N_C,\sigma}^{\dagger} \psi_{R\sigma} \right), \end{aligned} \quad (4)$$

$$\mathcal{H}_{\text{lead}} = \sum_{\nu=L,R} \sum_{k\sigma} \epsilon_{k\nu} c_{k\nu\sigma}^{\dagger} c_{k\nu\sigma}, \quad (5)$$

where $d_{i\sigma}$ annihilates an electron with spin σ at site i , and $n_{di} = \sum_{\sigma} d_{i\sigma}^{\dagger} d_{i\sigma}$. In the lead at ν ($= L, R$), the operator $c_{k\nu\sigma}^{\dagger}$ creates an electron with energy $\epsilon_{k\nu}$ corresponding to an one-particle state $\phi_{k\nu}(r)$. The hopping matrix elements v_L and v_R connect the chain and leads. At the interfaces, a linear combination of the conduction electrons $\psi_{\nu\sigma} = \sum_k c_{k\nu\sigma} \phi_{k\nu}(r_{\nu})$ mixed with the electrons at $i = 1$ or N_C (as illustrated in Fig. 1), where r_{ν} denotes the position at the interface in the lead side.

For this system, the Green's function is defined by

$$G_{jj'}(i\omega_n) = - \int_0^{\beta} d\tau \left\langle T_{\tau} d_{j\sigma}(\tau) d_{j'\sigma}^{\dagger}(0) \right\rangle e^{i\omega_n \tau}, \quad (6)$$

where $\beta = 1/T$, $d_{j\sigma}(\tau) = e^{\tau\mathcal{H}} d_{j\sigma} e^{-\tau\mathcal{H}}$, and $\langle \dots \rangle$ denotes the thermal average $\text{Tr} [e^{-\beta\mathcal{H}} \dots] / \text{Tr} e^{-\beta\mathcal{H}}$. We use units $\hbar = 1$. The corresponding retarded function, $G_{jj'}^{+}(\omega) = G_{jj'}(\omega + i0^{+})$, is obtained via the analytic continuation. Since the interaction U is finite only for the electrons in the chain at the center, the Dyson equation is written in the form

$$G_{ij}(z) = G_{ij}^0(z) + \sum_{i'j'=1}^{N_C} G_{i'i'}^0(z) \Sigma_{i'j'}(z) G_{j'j}(z). \quad (7)$$

Here $G_{ij}^0(z)$ is the unperturbed Green's function corresponding to $\mathcal{H}_0 \equiv \mathcal{H}_d + \mathcal{H}_{\text{lead}} + \mathcal{H}_{\text{mix}}$, and $\Sigma_{ij}(z)$ is the self-energy correction due to \mathcal{H}_U . Note that $G_{ij}(z) = G_{ji}(z)$, because of the time reversal symmetry of \mathcal{H} . The Dyson equation can be rewritten using $N_C \times N_C$ matrices $\mathbf{G}(z) = \{G_{ij}(z)\}$ and $\Sigma(z) = \{\Sigma_{ij}(z)\}$ as

$$\{\mathbf{G}(z)\}^{-1} = z \mathbf{1} - \mathbf{H}_C^0 - \mathbf{V}_{\text{mix}}(z) - \Sigma(z), \quad (8)$$

where

$$\mathbf{H}_C^0 = \begin{bmatrix} 0 & -t & & 0 \\ -t & 0 & \ddots & \\ & \ddots & \ddots & -t \\ 0 & & -t & 0 \end{bmatrix}, \quad (9)$$

$$\mathbf{V}_{\text{mix}}(z) = \begin{bmatrix} v_L^2 g_L(z) & 0 & & 0 \\ 0 & 0 & \ddots & \\ & \ddots & \ddots & 0 \\ 0 & 0 & v_R^2 g_R(z) & \end{bmatrix}, \quad (10)$$

and $g_{\nu}^{+}(\omega) \equiv \sum_k |\phi_{\nu\sigma}(r_{\nu})|^2 / (\omega - \epsilon_{k\nu} + i0^{+})$ is the Green's function at interface of the isolated lead. In the present study, we assume that the density of states is a constant, $g_{\nu}^{+}(\omega) = -i\pi\rho_{\nu}$, for small ω . Then the energy scale of the level-broadening becomes $\Gamma_{\nu} = \pi\rho_{\nu}v_{\nu}^2$, and it determines the two non-zero elements of $\mathbf{V}_{\text{mix}}^{+}(\omega)$.

2.1 Ground-state properties

If the ground state has a property $\text{Im} \Sigma^{+}(0) = 0$ at $T = 0$, the damping of the excitations at the Fermi level vanishes. Then the effective Hamiltonian defined by

$$\mathbf{H}_C^{\text{eff}} \equiv \mathbf{H}_C^0 + \text{Re} \Sigma^{+}(0) \quad (11)$$

plays a central role on the ground-state properties. It determines the renormalized hopping matrix elements $\mathbf{H}_C^{\text{eff}} = \{-\tilde{t}_{ij}\}$, and also the value of the Green's function at the Fermi level $\{\mathbf{G}^{+}(0)\}^{-1} = \mathbf{K}(0) - \mathbf{V}_{\text{mix}}^{+}(0)$, where

$$\mathbf{K}(\omega) \equiv \omega \mathbf{1} - \mathbf{H}_C^{\text{eff}}. \quad (12)$$

The determinant of the matrix $\{\mathbf{G}^{+}(0)\}^{-1}$ is related to the scattering matrix, and can be rewritten in the fol-

lowing form by expanding the first and N_C -th columns,

$$\begin{aligned} \det \{\mathbf{G}^+(0)\}^{-1} &= \left[-\Gamma_L \Gamma_R \det \mathbf{K}_{11}^{N_C N_C}(0) + \det \mathbf{K}(0) \right] \\ &+ i \left[\Gamma_L \det \mathbf{K}_{11}(0) + \Gamma_R \det \mathbf{K}_{N_C N_C}(0) \right]. \end{aligned} \quad (13)$$

Here $\mathbf{K}_{ij}(0)$ is a $(N_C - 1) \times (N_C - 1)$ derived from $\mathbf{K}(0)$ by deleting the i -th row and the j -th column. Similarly, $\mathbf{K}_{11}^{N_C N_C}(0)$ is a $(N_C - 2) \times (N_C - 2)$ matrix obtained from $\mathbf{K}(0)$ by deleting the first and the N_C -th rows, and the first and the N_C -th columns. At $T = 0$, the dc conductance is determined by the Green's function which connects the two leads, $g_{N_C} = (2e^2/h) 4\Gamma_R \Gamma_L |G_{N_C 1}^+(0)|^2$. It can also be expressed in terms of the scattering matrix

$$g_{N_C} = \frac{2e^2}{h} 4\Gamma_L \Gamma_R \frac{[\det \mathbf{K}_{11 N_C}(0)]^2}{\left| \det \{\mathbf{G}^+(0)\}^{-1} \right|^2}. \quad (14)$$

Furthermore at $T = 0$, the charge displacement can be determined by the Friedel sum rule,

$$\Delta N_{\text{tot}} = -\frac{2}{\pi} \text{Im} \log \left[\det \{\mathbf{G}^+(0)\}^{-1} \right]. \quad (15)$$

Particularly for the constant density of states, eq. (15) corresponds to the charge displacement defined by $\Delta N_{\text{tot}} = \sum_{i=1}^{N_C} \langle n_{d,i} \rangle$.²⁸ Recently, a related formulation which takes into account the self-energy corrections using the effective Hamiltonian has also been applied to a finite ring with a magnetic flux.²⁹

2.2 Conductance at half-filling

Specifically at half-filling $\epsilon_d = -U/2$, the matrix elements of $\mathbf{K}(0) = \{\tilde{t}_{ij}\}$ become zero for i and j belonging to the same sublattice, i.e., $|i - j| = 0, 2, 4, \dots$. Thus in this case, $\mathbf{K}(0)$ has a checkered structure, and it causes the even-odd dependence on the number of the interacting sites N_C .

For even N_C ($= 2M$), eq. (14) can be rewritten in the form

$$g_{2M} = \frac{2e^2}{h} \frac{\Gamma_L \Gamma_R \tilde{v}_C^2}{[(\Gamma_L \Gamma_R + \tilde{v}_C^2)/2]^2}, \quad (16)$$

$$\tilde{v}_C^2 = -\frac{\det \mathbf{K}(0)}{\det \mathbf{K}_{11}^{N_C N_C}(0)}, \quad (17)$$

where we have used the relations which can be deduced from the checkered structure of $\mathbf{K}(0)$: $\det \mathbf{K}_{N_C N_C}(0) = 0$, $\det \mathbf{K}_{11}(0) = 0$, and $[\det \mathbf{K}_{N_C 1}(0)]^2 = -\det \mathbf{K}(0) \det \mathbf{K}_{11}^{N_C N_C}(0)$. Specifically, for free electrons at $U = 0$, $\mathbf{K}(0)$ is given simply by $-\mathbf{H}_C^0$, and eq. (17) yields $\tilde{v}_C^2 = t^2$.

For odd N_C ($= 2M + 1$), the dc conductance, eq. (14), can be expressed as

$$g_{2M+1} = \frac{2e^2}{h} \frac{\tilde{\Gamma}_L \tilde{\Gamma}_R}{[(\tilde{\Gamma}_L + \tilde{\Gamma}_R)/2]^2}, \quad (18)$$

where $\tilde{\Gamma}_L = \lambda \Gamma_L$, $\tilde{\Gamma}_R = \Gamma_R / \lambda$, and

$$\lambda = \sqrt{\frac{\det \mathbf{K}_{11}(0)}{\det \mathbf{K}_{N_C N_C}(0)}}. \quad (19)$$

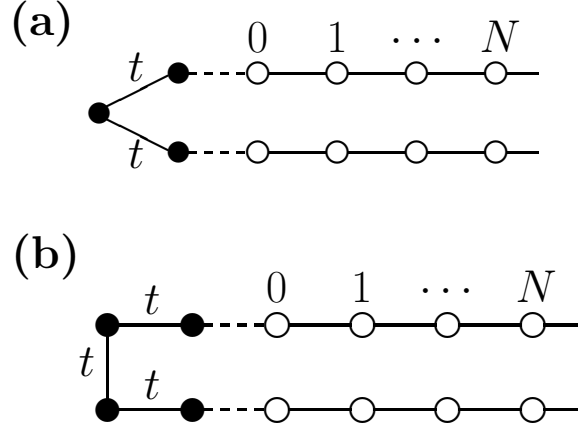


Fig. 2. Schematic pictures of discretized Hamiltonian for the NRG approach for (a) $N_C = 3$ and (b) $N_C = 4$

Here we have used the properties, $\det \mathbf{K}(0) = 0$, $\det \mathbf{K}_{11}^{N_C N_C}(0) = 0$, and $[\det \mathbf{K}_{N_C 1}(0)]^2 = \det \mathbf{K}_{11}(0) \det \mathbf{K}_{N_C N_C}(0)$. Especially, if the system has the inversion symmetry $\Gamma_L = \Gamma_R$ in addition to the electron-hole symmetry, the parameter defined in eq. (19) becomes $\lambda = 1$, and then the perfect transmission occurs, $g_{2M+1} = 2e^2/h$, for any value of M and U .

3. Fixed-point Hamiltonian and conductance

In the NRG method, the conduction band can be modelled by a linear chain as shown in Fig. 2, via a standard procedure of logarithmic discretization.^{21,22} Then, to capture the low-energy behavior correctly, we use a sequence of the Hamiltonian H_N defined by

$$H_N = \Lambda^{(N-1)/2} \left(\mathcal{H}_d + \mathcal{H}_U + H_{\text{mix}} + H_{\text{lead}}^{(N)} \right), \quad (20)$$

$$\begin{aligned} H_{\text{mix}} &= \bar{v}_L \sum_{\sigma} \left(f_{0,L\sigma}^{\dagger} d_{1,\sigma} + d_{1,\sigma}^{\dagger} f_{0,L\sigma} \right) \\ &+ \bar{v}_R \sum_{\sigma} \left(f_{0,R\sigma}^{\dagger} d_{N_C,\sigma} + d_{N_C,\sigma}^{\dagger} f_{0,R\sigma} \right), \end{aligned} \quad (21)$$

$$\begin{aligned} H_{\text{lead}}^{(N)} &= D \frac{1 + 1/\Lambda}{2} \sum_{\nu=L,R} \sum_{\sigma} \sum_{n=0}^{N-1} \xi_n \Lambda^{-n/2} \\ &\times \left(f_{n+1,\nu\sigma}^{\dagger} f_{n,\nu\sigma} + f_{n,\nu\sigma}^{\dagger} f_{n+1,\nu\sigma} \right), \end{aligned} \quad (22)$$

where D is the half-width of the conduction band. The hopping matrix elements \bar{v}_{ν} and ξ_n are defined by

$$\bar{v}_{\nu} = \sqrt{\frac{2D \Gamma_{\nu} A_{\Lambda}}{\pi}}, \quad A_{\Lambda} = \frac{1}{2} \frac{1 + 1/\Lambda}{1 - 1/\Lambda} \log \Lambda, \quad (23)$$

$$\xi_n = \frac{1 - 1/\Lambda^{n+1}}{\sqrt{1 - 1/\Lambda^{2n+1}} \sqrt{1 - 1/\Lambda^{2n+3}}}. \quad (24)$$

The factor A_{Λ} is needed to compare the discretized model with the original Hamiltonian eq. (1) precisely, and it behaves as $A_{\Lambda} \rightarrow 1$ in the continuum limit $\Lambda \rightarrow 1$.^{22,30} The low-lying energy states of the original Hamiltonian \mathcal{H} can be deduced from those of $\Lambda^{-(N-1)/2} H_N$ for large N .

In the following we concentrate on the case $\Gamma_L = \Gamma_R$ ($\equiv \Gamma$), where the couplings to the two leads are symmetric $\bar{v}_L = \bar{v}_R$ ($\equiv \bar{v}$). In the discretized Hamiltonian H_N in eq. (20), the matrix elements t and \bar{v} has multiplied by $\Lambda^{(N-1)/2}$. As shown in the next section, for large N the low-lying energy states of the many-body Hamiltonian H_N converge to the states which have one-to-one correspondence to the quasi-particles of a local Fermi liquid. It enables us to deduce the matrix elements of $\mathbf{H}_C^{\text{eff}}$, which are defined in Eq. (11), from the NRG spectrum.

At the fixed point, the low-energy spectrum of the many-body Hamiltonian H_N can be reproduced by the one-particle Hamiltonian consisting of $\mathbf{H}_C^{\text{eff}}$ and the two finite leads;

$$H_{\text{qp}}^{(N)} = \Lambda^{(N-1)/2} \left(\mathbf{H}_C^{\text{eff}} + H_{\text{mix}} + H_{\text{lead}}^{(N)} \right), \quad (25)$$

where $H_C^{\text{eff}} = -\sum_{ij=1}^{N_C} \tilde{t}_{ij} d_{i\sigma}^\dagger d_{j\sigma}$. It describes the free quasi-particles in the cluster with $N_C + 2(N+1)$ sites, and the corresponding Green's function can be written as

$$\begin{aligned} \{\mathbf{G}_{\text{qp}}(\omega)\}^{-1} &\equiv \\ \Lambda^{(N-1)/2} \left[\omega \Lambda^{-(N-1)/2} \mathbf{1} - \mathbf{H}_C^{\text{eff}} - \Lambda^{(N-1)/2} \mathbf{V}_{\text{mix}}^+(\omega) \right]. \end{aligned} \quad (26)$$

Here we have not included the renormalization factor $\partial\mathbf{\Sigma}/\partial\omega$, because at $T = 0$ it does not affect the dc conductance and charge displacement defined in eqs. (14) and (15). An eigenvalue ε^* of $H_{\text{qp}}^{(N)}$ satisfies the equation $\det\{\mathbf{G}_{\text{qp}}(\varepsilon^*)\}^{-1} = 0$, which can be written in a form similar to eq. (13),

$$\begin{aligned} \det \mathbf{K}_{11}^{N_C N_C}(\omega_N) [\bar{v}^2 \Lambda^{(N-1)/2} g_N(\varepsilon^*)]^2 + \det \mathbf{K}(\omega_N) \\ - [\det \mathbf{K}_{11}(\omega_N) + \det \mathbf{K}_{N_C N_C}(\omega_N)] [\bar{v}^2 \Lambda^{(N-1)/2} g_N(\varepsilon^*)] \\ = 0, \end{aligned} \quad (27)$$

where $\omega_N \equiv \varepsilon^* \Lambda^{-(N-1)/2}$. The Green's function $g_N(\omega)$ is introduced for an isolated lead with $N+1$ sites, and is defined with respect to the interface $n=0$. It can be expressed as $g_N(\omega) = \sum_{m=0}^N |\varphi_m(0)|^2 / (\omega - \epsilon_m)$, where ϵ_m and $\varphi_m(n)$ are the eigenvalue and eigenstate for the isolated lead. In the electron-hole symmetric case, Eq. (27) can be simplified by using the properties described in Sec. 2.2, as follows.

For even N_C ($= 2M$) and in the limit of large N , Eq. (27) yields

$$\left[\bar{v}^2 \lim_{N \rightarrow \infty} \Lambda^{(N-1)/2} g_N(\varepsilon^*) \right]^2 = - \frac{\det \mathbf{K}(0)}{\det \mathbf{K}_{11}^{N_C N_C}(0)}. \quad (28)$$

Thus, the parameter \tilde{v}_C^2 defined in eq. (17) can be related to the eigenvalue ε^* , as

$$\frac{\tilde{v}_C^2}{\Gamma^2} = \left(\frac{\bar{v}^2}{\Gamma D} \right)^2 \left[\lim_{N \rightarrow \infty} D \Lambda^{(N-1)/2} g_N(\varepsilon^*) \right]^2. \quad (29)$$

The prefactor in the right-hand side can also be written as $\bar{v}^2/(\Gamma D) = 2A_\Lambda/\pi$ by using eq. (23). Note the function, $\lim_{N \rightarrow \infty} \Lambda^{(N-1)/2} g_N(\omega)$, depends on whether N is even or odd. For even N_C , the fixed-point eigenvalue ε^*

depends on U/t and Γ/t , and the fixed-point Hamiltonian can be written in the form

$$H_{\text{qp}}^{(N)} = \sum_{\sigma} \sum_{l=1}^{N_{\text{qp}}} \varepsilon_l^* \left(\alpha_{l\sigma}^\dagger \alpha_{l\sigma} - \beta_{l\sigma}^\dagger \beta_{l\sigma} \right), \quad (30)$$

where $N_{\text{qp}} = N_C/2 + N + 1$. One can determine \tilde{v}_C^2/Γ^2 by substituting the value of ε_l^* deduced from the NRG results into eq. (29), and then the dc conductance can be obtained from eq. (16). Our formulation to deduce the conductance is analogous to the method used for the asymmetric Anderson impurity to determine the local charge from the fixed-point eigenvalue and Friedel sum rule.²³

The situation is quite different for odd N_C ($= 2M+1$). In this case, eq. (27) yields two separate branches of low-energy states for large N ,

$$\lim_{N \rightarrow \infty} \Lambda^{(N-1)/2} g_N(\varepsilon^*) = 0, \quad (31)$$

and

$$\left[\lim_{N \rightarrow \infty} \Lambda^{(N-1)/2} g_N(\varepsilon^*) \right]^{-1} = 0. \quad (32)$$

These can be deduced from the behavior of the determinants for small ω_N , $\det \mathbf{K}_{11}^{N_C N_C}(\omega_N) \propto \omega_N$ and $\det \mathbf{K}(\omega_N) \propto \omega_N$. These two branches imply that the eigenvalue ε^* does not depend on U , t and Γ . Specifically, eq. (31) corresponds to an isolated lead consisting of N sites starting from $n=1$ and ending at $n=N$, while eq. (32) corresponds to another lead with size $N+1$ that includes the site $n=0$. One way to interpret the fixed point is along the lines of the original work of Wilson,²¹ as a strong coupling fixed point, such that a single site at $n=0$ is removed from one of the leads to join the interacting sites and to form a singlet ground state for this cluster consisting of N_C+1 sites. However, here we derived eqs. (31) and (32) for the *connected* chain of $N_C+2(N+1)$ sites and have interpreted the fixed-point using the Hamiltonian $H_{\text{qp}}^{(N)}$, which is defined in eq. (25) and can be diagonalized as

$$H_{\text{qp}}^{(N)} = \sum_{\sigma} \varepsilon_0^* \alpha_{0\sigma}^\dagger \alpha_{0\sigma} + \sum_{\sigma} \sum_{l=1}^{N'_{\text{qp}}} \varepsilon_l^* \left(\alpha_{l\sigma}^\dagger \alpha_{l\sigma} - \beta_{l\sigma}^\dagger \beta_{l\sigma} \right), \quad (33)$$

where $\varepsilon_0^* = 0$ and $N'_{\text{qp}} = (N_C-1)/2 + N + 1$. This Hamiltonian links directly to the Fermi-liquid behavior, as the quasi-particles defined in this connected chain are in one-to-one correspondence with the single-particle excitations of the non-interacting system ($U=0$). This leads to more natural description for the ground state properties than the strong coupling interpretation which involves breaking the chain by effectively removing two sites.²⁷ As we show in the next section, the low-lying energy states of the many-body Hamiltonian H_N reproduce the energy spectrum determined by eqs. (31) and (32). The same behavior was seen in the single impurity case.^{21,22} Our numerical results confirm the Fermi-liquid behavior for $N_C=3$, and justify that the assumptions made in deducing the unitary-limit transport result, $g_{2M+1} = 2e^2/h$, for the case $N_C=3$.

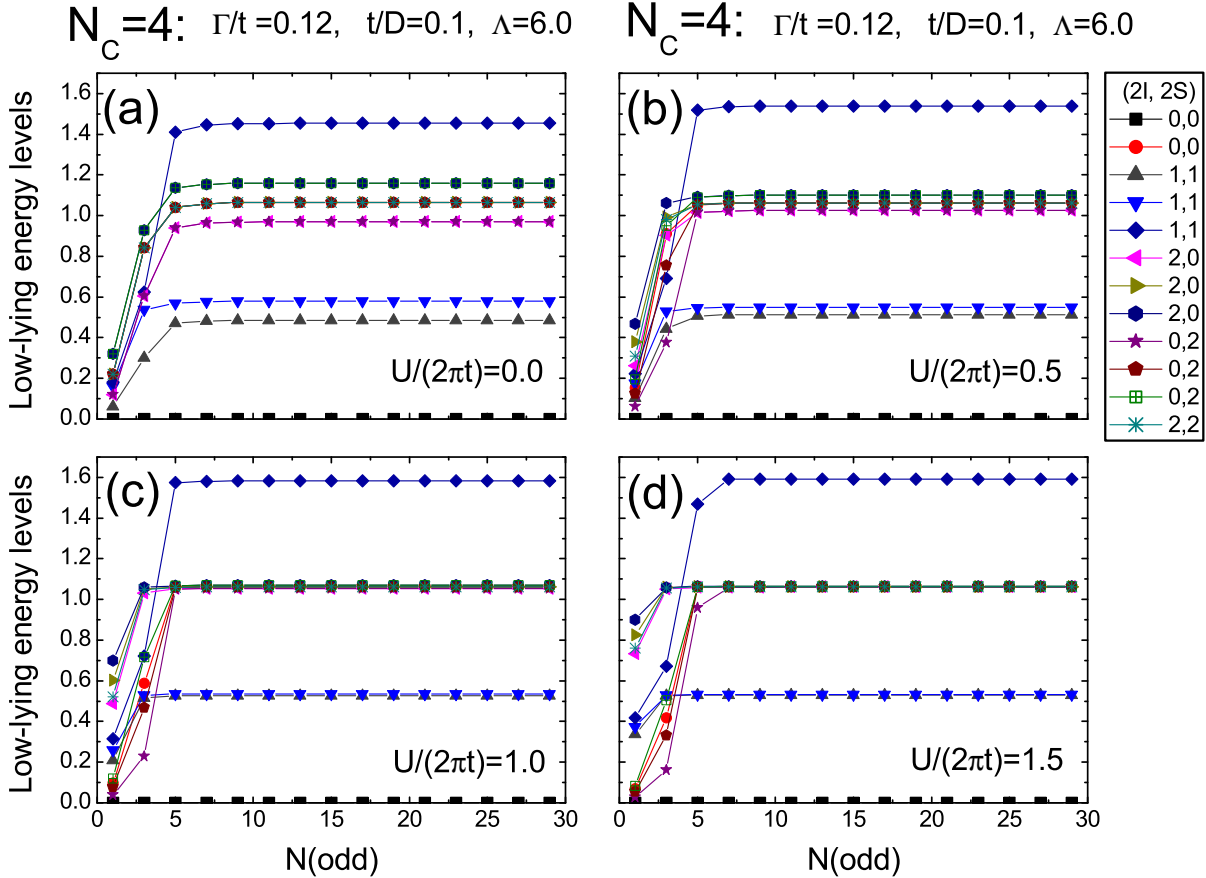


Fig. 3. Low-lying energy levels of H_N/D for $N_C = 4$ as a function of odd N (up to 29) for several values $U/(2\pi t)$: (a) 0.0, (B) 0.5, (c) 1.0, and (d) 1.5. Here $\epsilon_d = -U/2$, $\Gamma/t = 0.12$, $t/D = 0.1$ and $\Lambda = 6.0$. The eigenvalues are measured from the ground-state energy for each N . The label $(2I, 2S)$ corresponds to the total axial charge I and spin S . For $N \gtrsim 7$, the levels approach to the fixed point values.

4. NRG results

In the electron-hole symmetric case, the Hamiltonian H_N has a global $SU(2)$ symmetry of the axial charge,³¹ which is specified by the generators

$$\begin{aligned} \hat{I}_z &= \sum_{i=1}^{N_C} \frac{1}{2} \left(d_{i\uparrow}^\dagger d_{i\uparrow} + d_{i\downarrow}^\dagger d_{i\downarrow} - 1 \right) \\ &+ \sum_{\nu=L,R} \sum_{n=0}^N \frac{1}{2} \left(f_{n,\nu\uparrow}^\dagger f_{n,\nu\uparrow} + f_{n,\nu\downarrow}^\dagger f_{n,\nu\downarrow} - 1 \right), \end{aligned} \quad (34)$$

$$\hat{I}_+ = \sum_{i=1}^{N_c} (-1)^i d_{i\uparrow}^\dagger d_{i\downarrow}^\dagger + \sum_{\nu=L,R} \sum_{n=0}^N (-1)^{\theta_{n\nu}} f_{n,\nu\uparrow}^\dagger f_{n,\nu\downarrow}^\dagger, \quad (35)$$

$$\hat{I}_- = \sum_{i=1}^{N_c} (-1)^i d_{i\downarrow}^\dagger d_{i\uparrow}^\dagger + \sum_{\nu=L,R} \sum_{n=0}^N (-1)^{\theta_{n\nu}} f_{n,\nu\downarrow}^\dagger f_{n,\nu\uparrow}^\dagger. \quad (36)$$

Here $\theta_{n,L} \equiv -n$ for the left lead, and $\theta_{n,R} \equiv N_C + n + 1$ for the right lead, so that the factor $(-1)^{\theta_{n\nu}}$ becomes $+1$ or -1 depending on whether the site labeled by (n, ν) is in an even or odd sublattice. The z component of the axial charge corresponds to the total charge, $\hat{Q} = 2\hat{I}_z$. Furthermore, the operators \hat{I}_z and \hat{I}_\pm satisfy

the commutation relations identical to those of the total spin operators \hat{S}_z and \hat{S}_\pm . Thus, using the symmetry of $SU(2)_{\text{spin}} \times SU(2)_{\text{axial}}$, the eigenstates can be classified according to the quantum numbers for the operators \hat{S}_z , \hat{S}^2 , \hat{I}_z , and $\hat{I}^2 \equiv \hat{I}_z^2 + (\hat{I}_+ \hat{I}_- + \hat{I}_- \hat{I}_+)/2$, as

$$H_N |I, I_z, S, S_z; r\rangle_N = E_{N,I,S,r} |I, I_z, S, S_z; r\rangle_N. \quad (37)$$

The use of the $SU(2)_{\text{spin}} \times SU(2)_{\text{axial}}$ symmetry has a great numerical advantage [see also, Appendix]. One can save the eigenstates to be retained in the process of the NRG iteration. Particularly in the multi-channel systems, such as the one we are considering (2-channel in our case), the number of low-energy states to be retained increases exponentially with the number of the channels. Thus the reduction of the Hilbert space helps to improve the numerical accuracy. After using the two $SU(2)$ symmetries, we have retained typically 1000 low-energy states in the NRG calculations for the Hubbard model with $N_C = 3$ and 4. Under this condition the truncation occurs first at $N = 2$, namely H_N has been diagonalized exactly up to $N = 1$ where the total number of the sites in the cluster is 7 and 8 for $N_C = 3$ and 4, respectively, as shown in Fig. 2. Since two new sites at $n = N + 1$ are included in each step of the recursive procedure, the dimension of Hilbert space becomes typically 4^2 larger than the number of the states retained in the previous step apart from some reductions due to

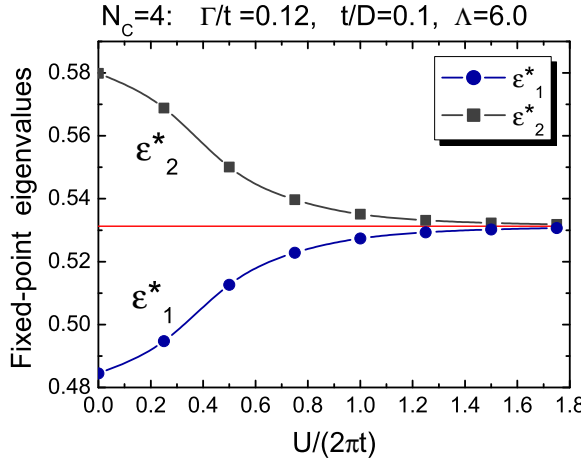


Fig. 4. The U -dependence of ε_1^* and ε_2^* for the 4-site Hubbard model for odd N . For large U , these two approach to a single value 0.5312, which corresponds to the lowest pole of the Green's function of the isolated lead, $\lim_{N \rightarrow \infty} \Lambda^{(N-1)/2} g_N(\omega)$, for odd N .

the symmetries. To overcome the influence of the truncation, which starts not so far from the interacting region, we have concentrated on the case in which Γ/t is small ($\simeq 0.1$) and have used a rather large value for the discretization parameter $\Lambda = 6.0$. The hopping matrix between the interacting sites has taken to be $t/D = 0.1$ in the calculations.

The use of an additional inversion symmetry $\Gamma_L = \Gamma_R$ does not change the total number of the basis states to be retained in the interacting case $U \neq 0$, although each subspace labeled by I and S can be divided up into two segments. The inversion symmetry can be employed by introducing the bonding and antibonding orbits $a_{n,\pm,\sigma} = (f_{n,R,\sigma} \pm f_{n,L,\sigma})/\sqrt{2}$. However, for even N_C these orbits make the axial charge nonlocal, while the locality is preserved for odd N_C . We have also performed the calculations using these orbits for odd N_C . It makes the computer time somewhat shorter, but is not essential for improving the numerical accuracy.

4.1 Results for $N_C = 4$

We first of all consider the Hubbard chain of the size $N_C = 4$, which can be regarded as a simplest case for an even interacting chain. In Fig. 3, the low-lying energy levels of H_N for $\Gamma/t = 0.12$ are plotted as a function of odd N , where $N + 1$ is even, for several values of the Coulomb interaction: $U/(2\pi t) = 0.0, 0.5, 1.0$, and 1.5 . The eigenvalues are measured from the ground-state en-

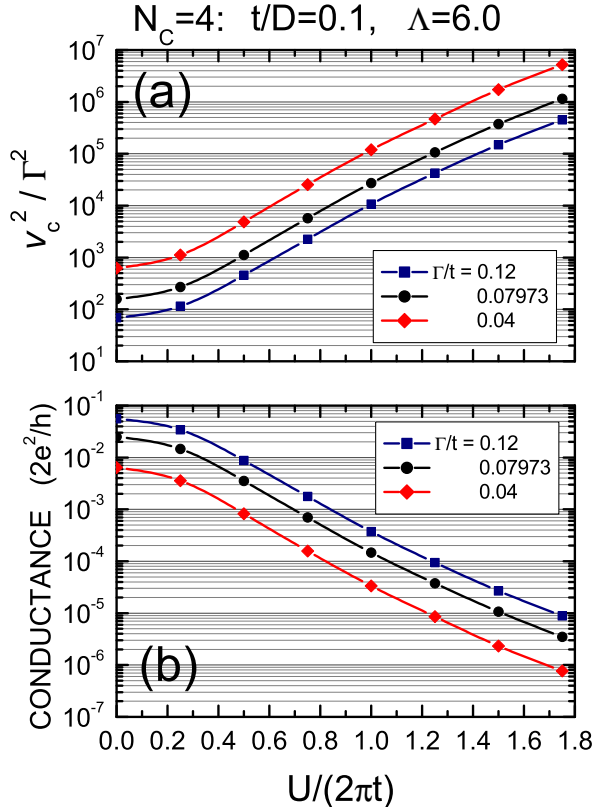


Fig. 5. The U -dependence of (a) \tilde{v}_C^2 and (b) the dc conductance g_{N_C} for the 4-site Hubbard model for several values of the hybridization: $\Gamma/t = 0.04, 0.07973$, and 0.12 . The parameter \tilde{v}_C^2 is deduced from the fixed-point eigenvalue ε_l^* by using eq. (29).

ergy for each N . The flow of the energy levels converges to the fixed-point values for $N \gtrsim 10$ in these examples. In the case of even N_C , the fixed-point eigenvalues depend on U and Γ . The numerical results for the many-body low-lying states can be compared with the quasi-particle eigenstates defined in eq. (30). We found that the many-body eigenvalues E_i^* of H_N shown in Fig. 3 have correspondence to the excited states described by the quasi-particles with the energy ε_i^* , as summarized in Table I. The first two excitation energies of H_N , i.e., E_1^* and E_2^* , determine the two *one-particle* energies ε_1^* and ε_2^* , respectively. The many-body eigenvalues above these two, E_3^*, E_4^*, \dots , agree well with those calculated from ε_1^* and ε_2^* with the assignments given in the table I. We have confirmed that the two quantum numbers, the total axial charge I and spin S , for the low-energy eigenstates are consistent with these assignments. This feature of the low-lying energy states is similar to that for the Kondo and Anderson models,^{21,22} and means that the low-energy properties can be described by the local Fermi-liquid theory. Specifically, for even N_C , the fixed-point Hamiltonian $H_{qp}^{(N)}$ defined in eq. (25) can be separated into a couple of the chains when the system has an inversion symmetry, and each of the chains can be mapped onto a noninteracting version of the asymmetric Anderson model.²³ In Fig. 4, the U dependence of ε_1^* and ε_2^* are shown for the parameter set; $\Gamma/t = 0.12$,

E_1^*	$= \varepsilon_1^*$
E_2^*	$= \varepsilon_2^*$
E_3^*	$= 2\varepsilon_1^*$
E_4^*	$= \varepsilon_1^* + \varepsilon_2^*$
E_5^*	$= 2\varepsilon_2^*$
E_6^*	$= 3\varepsilon_1^*$

Table I. Low-lying fixed-point eigenvalues of H_N for $N_{HUB} = 4$, for odd N .

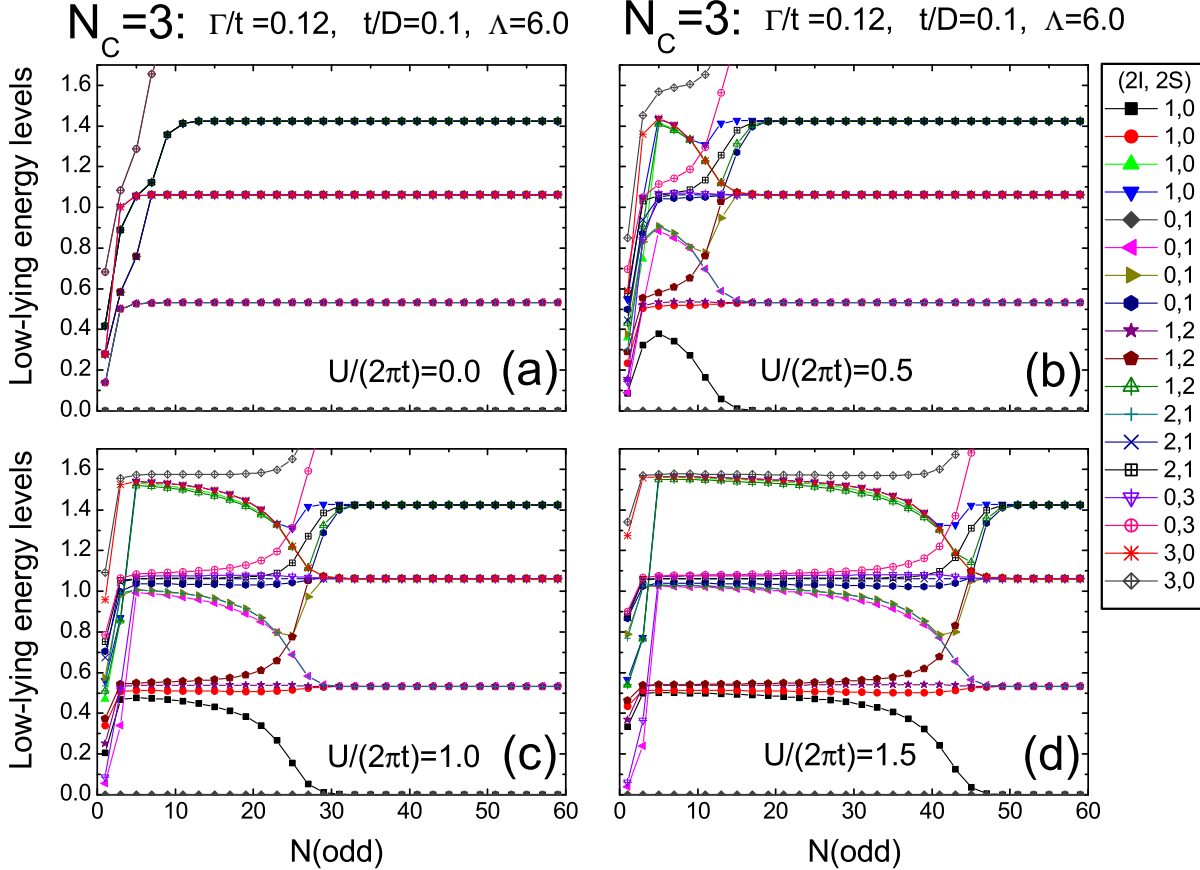


Fig. 6. Low-lying energy levels of H_N/D for $N_C = 3$ as a function of odd N (up to 59) for several values $U/(2\pi t)$: (a) 0.0, (b) 0.5, (c) 1.0, and (d) 1.5. Here $\epsilon_d = -U/2$, $\Gamma/t = 0.12$, $t/D = 0.1$ and $\Lambda = 6.0$. The eigenvalues are measured from the ground-state energy for each N . The label $(2I, 2S)$ corresponds to the total axial charge I and spin S . The size of the lead, N^* , required to get the energy levels closed to the fixed-point values increases with U .

$t/D = 0.1$, and $\Lambda = 6$. The difference between ε_1^* and ε_2^* decreases with increasing U . This tendency links with the behavior of the other excitation energies shown in Fig. 3, namely E_3^* , E_4^* , and E_5^* become close to each other with increasing U . For large U , both ε_1^* and ε_2^* approach to 0.5312 which corresponds to the smallest pole of $\lim_{N \rightarrow \infty} \Lambda^{(N-1)/2} g_N(\omega)$ for odd N . It means that in the limit of $U \rightarrow \infty$ the low-energy states are determined by those of the isolated leads.

Substituting the value of ε_1^* or ε_2^* into eq. (29) and taking $N = 99$ for the Green's function of the isolated lead, we obtain the parameter \tilde{v}_C defined in eq. (17), and then determine the dc conductance via eq. (16). The results are plotted against $U/(2\pi t)$ in Fig. 5 for several values of hybridization; $\Gamma/t = 0.04$, 0.07973, and 0.12. The value of \tilde{v}_C determined from ε_1^* agree with that determined from ε_2^* . Furthermore, we have also calculated \tilde{v}_C using the fixed-point eigenvalues for even N and the Green's function $\Lambda^{(N-1)/2} g_N(\omega)$ for $N = 100$. The result again agrees with that deduced from the data for odd N . The parameter \tilde{v}_C increases with the Coulomb interaction U reflecting the behavior of the fixed-point eigenvalue shown in Fig. 4. The results for the conductance are plotted in Fig. 5 (b). When the coupling with leads Γ increases, the conductance also increases in the parameter region we have examined. For large U , the

conductance decreases exponentially with increasing U . This can be understood as a tendency towards the development of a Mott insulator gap. Namely, for large even N_C , the conductance is expected to show a behavior $g_{N_C} \propto e^{-N_C/\xi}$, where $\xi \sim \hbar v_F / \Delta_{\text{gap}}$ is a correlation length determined by the Hubbard gap Δ_{gap} and Fermi velocity v_F . This is because $\Delta_{\text{gap}} \propto U$ for large U , as can be seen in the Bethe ansatz results for one-dimensional Hubbard model.³² Our previous results obtained with the 2nd order perturbation theory in U are valid qualitatively.¹³ However, the 2nd-order perturbation theory fails to reproduce the correct exponential dependence for large U , and which can however be obtained using the non-perturbative NRG technique.

4.2 Results for $N_C = 3$

We next consider the Hubbard chain with the odd number of interacting sites. In Fig. 6, the flow of the low-lying eigenvalues of H_N/D for $N_C = 3$ is plotted as a function of odd N for several values of the Coulomb interaction $U/(2\pi t) = 0.0, 0.5, 1.0$, and 1.5 . The flow of the eigenvalues of H_N/D is quite different from that for even N_C . In the case of odd N_C , a number of noninteracting sites in the leads is required to reach the fixed point that determines the low-energy properties. The number of NRG iterations N^* that is needed to get the conver-

E_1^*	ε_1^*
E_2^*	$2\varepsilon_1^*$
E_3^*	ε_2^*
E_4^*	$3\varepsilon_1^*$
E_5^*	$\varepsilon_1^* + \varepsilon_2^*$
E_6^*	$4\varepsilon_1^*$

Table II. Low-lying fixed-point eigenvalues of H_N for $N_{\text{HUB}} = 3$.

gent results increases with U , and in the case of Fig. 6 it is estimated to be (b) $N^* \simeq 15$, (c) $N^* \simeq 30$, and (d) $N^* \simeq 50$. It means that there is a characteristic energy scale determined by $T^* \simeq D\Lambda^{-(N^*-1)/2}$, where the factor $\Lambda^{-(N^*-1)/2}$ is introduced to recover the original energy scale from H_N defined in eq. (20). This characteristic energy scale is determined by width of the Kondo resonance, $T^* \sim T_K$, appearing at the Fermi level.

For $N \gtrsim N^*$, the fixed-point eigenvalues do not depend on U and agree with those of the the noninteracting leads determined by eqs. (31) and (32). Namely, these low-lying many-body states, E_i^* , have the one-to-one correspondence with the quasi-particle states described by eq. (33). The precise correspondence is summarized in Table II, and these assignments coincide with those for the single Anderson impurity.²² The first and third excited states, E_1^* and E_3^* , correspond to the first two *one-particle* states, the energy of which are given by $\varepsilon_1^* = 0.53124$ and $\varepsilon_2^* = 1.42546$. We have also confirmed for $N_C = 3$ that the fixed-point eigenvalues at $N \gtrsim N^*$ do not depend on whether N is even or odd. These feature show that the low-temperature properties at $T \lesssim T^*$ can described by the quasi-particles of the local Fermi theory, and it justifies the assumptions made in deducing the unitary-limit conductance, $g_{N_C} = 2e^2/h$, at $T = 0$ for odd N_C .

To capture the low-energy Kondo behavior at $T \lesssim T_K$ correctly, one needs to repeat the NRG iterations up to $N \gtrsim N^*$ as mentioned in the above. In other words, a sufficiently large number of the noninteracting sites are required for the reservoirs to make the finite-size energy separation smaller than T^* , and a similar notice has recently been emphasized by several authors.^{33,34} From the results obtained for a small cluster with size corresponding to $N \lesssim N^*$, it is still possible to deduce the high-temperature properties at $T \gtrsim T_K$.^{35,36} In the NRG method the logarithmic discretization of the conduction band, eq. (20), yields the hopping matrix element that decreases exponentially with increasing N ,^{21–23} and it makes the convergence to the fixed point efficient.

5. Discussion and Summary

In the present work, we have clarified the difference in the transport properties between the Hubbard chain of even and odd N_C . Then, what happens in the limit of large N_C ? It might sound somewhat puzzling since the ground state of the Hubbard chain is an insulating state in the thermodynamic limit. However, the existence of the energy scale $T^* \sim T_K$ for odd N_C brings us the answer. For odd N_C ($= 2M + 1$), there is the Kondo resonance at the Fermi level. The width T_K decreases

with N_C increases, and finally $T_K \rightarrow 0$ in the limit of $N_C \rightarrow \infty$ because the Hubbard gap Δ_{gap} evolving with increasing N_C disturbs the electrons to screen the local moment. Thus, the value of the conductance g_N depends on the order of taking the limits of $N_C \rightarrow \infty$ and $T \rightarrow 0$. For finite N_C , the Kondo behavior at $T < T_K$ causes the unitary-limit behavior

$$\lim_{M \rightarrow \infty} \left[\lim_{T \rightarrow 0} g_{2M+1} \right] = 2e^2/h. \quad (38)$$

In contrast, when the thermodynamic limit $N_C \rightarrow \infty$ is taken first at small but finite T , the conductance must be determined by the Mott-Hubbard behavior at $T > T_K$, as

$$\lim_{T \rightarrow 0} \left[\lim_{M \rightarrow \infty} g_{2M+1} \right] = 0. \quad (39)$$

Therefore, in order to observe the unitary-limit behavior at an accessible temperature, the number of the interacting sites N_C should not be so large. For even N_C ($= 2M$) there is no Kondo resonance at Fermi level, and the conductance does not depend on the limiting procedure

$$\lim_{\substack{M \rightarrow \infty \\ T \rightarrow 0}} g_{2M} = 0. \quad (40)$$

The two limits, $N_C \rightarrow 0$ and $T \rightarrow 0$, considered here are analogous to the $k \rightarrow 0$ and $\omega \rightarrow 0$ limits of the vertex corrections for the interacting Fermi systems with the translational invariance.³⁷

In summary, we have studied the conductance through a finite Hubbard chain of the size N_C connected to two noninteracting leads using the NRG method. The results show that the low-lying energy states can be described by the quasi-particles of a local Fermi liquid. We have also presented a formulation for deducing the dc conductance from the fixed-point Hamiltonian. The results of the conductance for even N_C show the expected exponential decay as a function of U at half-filling.

Acknowledgements

One of us (AO) wishes to acknowledge the support by the Grant-in-Aid for Scientific Research from JSPS. ACH wishes to thank the EPSRC(Grant GR/S18571/01) for financial support. Numerical computation was partly performed at Yukawa Institute Computer Facility.

Appendix: Reduced matrix element

In the electron-hole symmetric case, the Wigner-Eckart theorem for the spin and axial charge $SU(2)_{\text{spin}} \times SU(2)_{\text{axial}}$ yields

$$\begin{aligned} & \langle I, I_z, S, S_z; r | f_{n\sigma}^\dagger | I', I'_z, S', S'_z; r' \rangle \\ &= \langle S', S'_z; 1/2, \sigma | S, S_z \rangle \langle I', I'_z; 1/2, 1/2 | I, I_z \rangle \\ & \quad \times F_n(I, S; r | I', S'; r'), \end{aligned} \quad (\text{A.1})$$

where the Clebsh-Gordan coefficient appears for the total spin $\langle S', S'_z; 1/2, \sigma | S, S_z \rangle$ and for the total axial charge $\langle I', I'_z; 1/2, 1/2 | I, I_z \rangle$. The invariant matrix element $F_n(\alpha' | \alpha)$ has the following properties against the

exchange of the arguments α' and α ;

$$\begin{aligned} F_n(I, S - 1/2; r' | I - 1/2, S; r) \\ = (-1)^n \sqrt{\frac{2S+1}{2S}} \sqrt{\frac{2I}{2I+1}} \\ \times F_n(I - 1/2, S; r | I, S - 1/2; r'), \end{aligned} \quad (A.2)$$

$$\begin{aligned} F_n(I, S + 1/2; r' | I - 1/2, S; r) \\ = (-1)^{n+1} \sqrt{\frac{2S+1}{2S+2}} \sqrt{\frac{2I}{2I+1}} \\ \times F_n(I - 1/2, S; r | I, S + 1/2; r'). \end{aligned} \quad (A.3)$$

- 1) L. I. Glazman and M. E. Raikh: JETP Lett. **47** (1988) 452.
- 2) T. K. Ng and P. A. Lee: Phys. Rev. Lett. **61** (1988) 1768.
- 3) D. Goldhaber-Gordon, H. Shtrikman, D. Mahalu, D. Abusch-Magder, U. Meirav, and M. A. Kastner: Nature **391** (1998) 156.
- 4) S. M. Cronenwett, T. H. Oosterkamp, and L. P. Kouwenhoven: Science **281** (1998) 540.
- 5) W. Hofstetter, J. König, and H. Schoeller: Phys. Rev. Lett. **87** (2001) 156803.
- 6) K. Kobayashi, H. Aikawa, S. Katsumoto, and Y. Iye: Phys. Rev. Lett. **88** (2002) 256806.
- 7) A. Oguri, Y. Tanaka, and A. C. Hewson: J. Phys. Soc. Jpn. **73** (2004) 2494.
- 8) C. L. Kane and M. P. A. Fisher: Phys. Rev. Lett. **68** (1992) 1220.
- 9) S. Tarucha, T. Honda, and T. Saku: Solid State Commun. **94** (1995) 413.
- 10) V. Meden and U. Schollwöck: Phys. Rev. B **67** (2003) 193303; V. Meden, S. Andergassen, W. Metzner, U. Schollwöck and K. Schönhammer: Europhys. Lett. **64** (2003) 769; T. Ens, V. Meden, S. Andergassen, W. Metzner: X. Barnabé-Thériault and K. Schönhammer, cond-mat/0411310.
- 11) R. A. Molina, D. Weinmann, R. A. Jalabert, G.-L. Ingold, and J. -L. Pichard: Phys. Rev. B **67** (2003) 235306; R. A. Molina,

- D. Weinmann, and J. -L. Pichard: Europhys. Lett. **67** (2004) 96.
- 12) A. Oguri: Phys. Rev. B **59** (1999) 12240.
- 13) A. Oguri: Phys. Rev. B **63** (2001) 115305; *ibid.* [Errata: **63** (2001) 249901].
- 14) A. Oguri: J. Phys. Soc. Jpn. **70** (2001) 2666; *ibid.* **72**, 3301 (2003).
- 15) A. Oguri: J. Phys. Soc. Jpn. **66** (1997) 1427.
- 16) J. S. Langer and V. Ambegaokar, Phys. Rev. **121** (1961) 1090.
- 17) K. Yamada: Prog. Theor. Phys. **53** (1975) 970; *ibid.* **54** (1975) 316; K. Yosida and K. Yamada: *ibid.* **53** (1975) 1286.
- 18) V. Zlatić and V. Horvatić: Phys. Rev. B **28** (1983) 6940.
- 19) N. Kawakami and A. Okiji: Solid State Commun. **43** (1982) 467.
- 20) B. Wiegman and A. M. Tsvelick: J. Phys. C **16** (1983) 2281.
- 21) K. G. Wilson: Rev. Mod. Phys. **47** (1975) 773.
- 22) H. R. Krishna-murth, J. W. Wilkins: and K. G. Wilson, Phys. Rev. B **21** (1980) 1003.
- 23) H. R. Krishna-murth, J. W. Wilkins: and K. G. Wilson, Phys. Rev. B **21** (1980) 1044.
- 24) W. Izumida, O. Sakai, and Y. Shimizu: J. Phys. Soc. Jpn. **66** (1997) 717; J. Phys. Soc. Jpn. **67** (1998) 2444.
- 25) W. Izumida and O. Sakai: Phys. Rev. B **62** (2000) 10260.
- 26) A. C. Hewson: J. Phys.: Condens. Matter **13** (2001) 10011.
- 27) A. C. Hewson, A. Oguri, and D. Meyer: Eur. Phys. J. B **40** (2004) 177; A. C. Hewson: to appear in J. Phys. Soc. Jpn. suppl. (2005).
- 28) Yoshihide Tanaka, A. Oguri, and H. Ishii: J. Phys. Soc. Jpn. **71** (2002) 211.
- 29) T. Rejec and A. Ramašak: Phys. Rev. B **68** (2003) 035342; *ibid.* **68** (2003) 033306.
- 30) O. Sakai, Y. Shimizu, and T. Kasuya: Prog. Theor. Phys. Suppl. **108** (1992) 73.
- 31) D. L. Cox and A. Zawadowski: Adv. Phys. **47** (1998) 599.
- 32) E. H. Lieb and R. Y. Wu: Phys. Rev. Lett. **20** (1968) 1445.
- 33) J. Bonča, A. Ramašak and T. Rejec: cond-mat/0407590.
- 34) P. S. Cornaglia, and D. R. Grempel: cond-mat/0408168.
- 35) G. Chiappe and J. A. Vergés: J. Phys.: Condens. Matter **15** (2003) 8805.
- 36) C. A. Büsser, A. Moreo, and E. Dagotto: Phys. Rev. B **70** (2004) 035402.
- 37) A. A. Abrikosov, L. P. Gor'kov, and I. Y. Dzyaloshinskii: *Quantum Field Theoretical Methods in Statistical Physics* (Pergamon, London, 1965).